Power Engineering and Engineering Thermophysics
https://www.acadlore.com/journals/PEET

Engine Exhaust Stub Sizing for Turboprop Powered Aircraft

Chikkanayakanahalli Anand Vinay[1*], Kumar Gottegere Narayanappa[2], Girdharababu Yepuri[3]

[1] C-CADD, CSIR-NAL, HAL Airport Road, 560017 Bangalore, India
[2] Mechanical Engineering Department, National Institute of Technology-Surathkal, 575025 Mangalore, Karnataka, India
[3] PRD, CSIR-National Aerospace Laboratories, 560017 Bangalore, India

[*] Correspondence: Chikkanayakanahalli Anand Vinay (vinay.ca@nal.res.in)

Received: 12-12-2022 **Revised:** 01-11-2023 **Accepted:** 02-20-2023

Citation: C. A. Vinay, K. G. Narayanappa, and G. Yepuri, "Engine exhaust stub sizing for turboprop powered aircraft," *Power Eng. Eng Thermophys.*, vol. 2, no. 1, pp. 49-56, 2023. https://doi.org/10.56578/peet020105.

Abstract: Turboprop engines are widely used in the commuter or light transport aircraft (LTA) turboprop engines, because they are more fuel efficient than the propeller, which has a low jet velocity, at flight velocities below 0.6 Mach. For short distances, turboprop engines are more fuel efficient than jet engines, because the light weight assures a high power output per unit of weight. In addition, turboprops are known for their efficiency at medium and low altitudes. Turboprop engines require an exhaust stub (or nozzle) to duct the engine exhaust flue gas outboard of the aircraft. The design of these exhaust stubs is dictated primarily by the aircraft configuration. During the exhaust stub design, full flow at bends and in diffusing sections must be realized by following the established practice for the design of internal flow ducts. Otherwise, the flow will separate from the wall, causing unnecessary pressure loss and reducing the effective flow area. This paper discusses some of the many variations in exhaust stub design, and examines how they influence the performance of the engine, the performance of the aircraft, and the manufacturing aspect. The authors carried out a detailed analysis on the influencing parameters, such as the location, orientation, flange dimension, and geometric effective area of exhaust port. On this basis, the authors determined the jet temperature at exhaust stub exit and temperature at exhaust stub exit plane and nacelle midsection were determined at both static and cruise condition, laying the data basis for further analysis on the exhaust temperature effects over the nacelle and aircraft surfaces.

Keywords: Exhaust stub; Turboprop; Nacelle; Plume; Light Transport Aircraft (LTA)

1. Introduction

Turboprop engines require an exhaust stub (nozzle) to duct the engine exhaust gas outboard of the aircraft. The exhaust stub design is dictated primarily by the aircraft configuration, and therefore determined by the aircraft manufacturer. This paper summarizes the typical methodology of exhaust stub design for turboprop engines, and investigates the effects of the exhaust system on overall engine performance. Typically, the turboprop engine is fitted with a twin-port exhaust case. As part of the ports, flanges are where the exhaust stubs are directly attached, and duct the exhaust gases out of the aircraft. The flange area of the engine is fixed by the engine manufacturer.

During the exhaust stub design, full flow at bends and in diffusing sections must be realized by following the established practice for the design of internal flow ducts. Otherwise, the flow will separate from the wall, causing unnecessary pressure loss and reducing the effective flow area. The turboprop engine is mainly powered by the shaft power and the exhaust thrust [1, 2]. The distribution of power between shaft and the exhaust is governed directly by the exit area of the exhaust nozzle.

The selection of the exit area of the exhaust nozzle is a trade-off between take-off and cruise requirements. At take-off conditions, a large exit area is advantageous, for exhaust stub thrust contributes less to the total propulsive thrust. At cruise conditions, however, the exhaust stub thrust can be effectively recovered, making it possible to optimize the equivalent shaft horsepower (ESHP) and reduce the exhaust stub drag.

Figure 1 shows the main influencing parameters of the exhaust stub for a aircraft engine. Figure 2 presents the location, orientation, and flange dimensions of exhaust ports. The geometric effective area of the ports stands at 93 in^2.

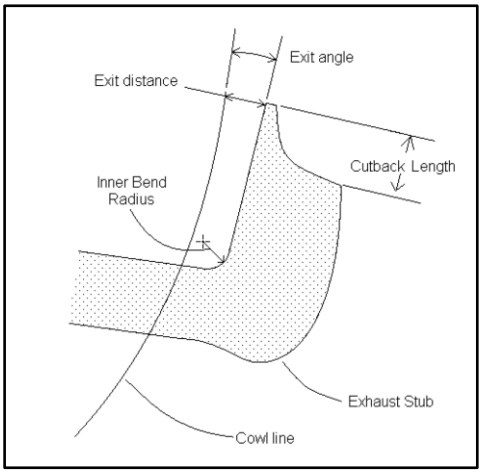

Figure 1. Main parameters of the exhaust stub

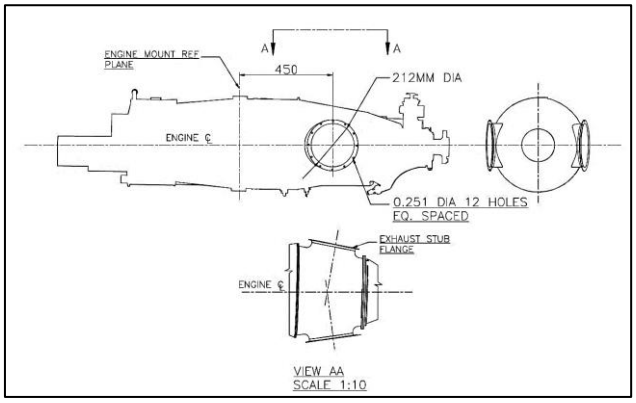

Figure 2. Location of twin exhaust ports of turboprop engine

The following issues should be considered to design effective exhaust stubs: Selecting an effective exit area of the stub; maximizing the thrust recovery and minimizing external aerodynamic drag by turning the stubs; reducing potential problems arising from overheating of aircraft surfaces and sooting through the management of the exhaust plume trajectory.

To enhance ram recovery and reduce drag, Kong [3] explored how to integrate turboprop engines with engine cooling systems, exhaust-duct, and engine-fuselage systems. To achieve the discharge coefficient (Cd) of 0.85 at cruising, the exhaust duct throat area was reduced from 74 square inches to 56 square inches. The sooting of the fuselage was avoided by keeping a discharge angle of 12 degrees and a 4-inch clearance.

Stalewski [4] developed and optimized the exhaust system for light turboprop aircraft (LTA). The design of the exhaust system, which disperses exhaust gases potentially far from the aircraft, was the goal of the optimization process, particularly during a descent flight. The turboprop engine's primary role is to remove exhaust, but it also helps cooling of the engine bay. The use of URANS solver-based ANSYS FLUENT software allows for the three-dimensional analysis of flow inside the exhaust system (including the effect of the propeller) and surrounding the aircraft.

The SST k-ω model is suitable for predicting the flow behavior in regions away from the wall. This two-equation eddy-viscosity model hybridizes the Wilcox k-omega and the k-epsilon models, which are widely adopted in aerodynamic applications. In the SST k-ω model, a blending function is employed to activate the Wilcox model near the wall and the k-epsilon model in the free stream. The turbulent viscosity formula is modified to account for the transport effects of the principal turbulent shear stress [5, 6].

In general, the k-ω SST model can accurately predict the onset and the size of separation under negative pressure gradient, and can be improved into the k-ω turbulence models for aerodynamics applications. The commercially available software ANSYS-FLUENT [7], which is based on finite-volume method, can be utilized to solve the three-dimensional flow over the airframe and propeller, using Reynolds-Averaged Navier-Stokes equations. The k-ω SST model can also be adapted, so that the governing equations can be spatially discretized by a second-order upwind scheme. The pressure-velocity coupling can be achieved by the SIMPLE scheme, coupled with a double-precision arithmetic scheme [8].

The exhaust system can be designed and optimized through parametric design methodology. Specifically, the parametric model can be established on the in-house software PARADES, which adopts the Non-Uniform Rational B-Splines (NURBS) representation of parameterized objects. The design criteria can be formulated based on the properties of the airflow outside, around, and inside the aircraft. The aerodynamics can be analyzed by the CFD-software package. The Navier Stokes equations, along with the virtual blade model (VBM) can be employed to simulate the rotating propeller. Thus, the time-averaged aerodynamic effects of rotating blades can be modelled using momentum source terms placed inside fluid-disk zone. The source terms can be computed based on the blade element theory. In this way, it is possible to evaluate how the changing design parameters (direction, length or diameter of the exhaust channels) affect the alleviation of negative effects from exhaust gas propagation.

Mali et al. [9] numerically optimized the exhaust system, and estimated the exhaust jet impingement on the propeller and on the aft nacelle surfaces, with the aid of the RANS-based k-epsilon model in ANSYS FLUENT. According to the velocity magnitude along the cut plane for both actual and optimized stubs, the exhaust gas comes from stub and gets mixed with the outer air due to the rotating propeller. A high velocity region was observed at downstream side of propeller, suggesting that the propeller develops a huge thrust. It can be observed that, the temperature of the optimized stub increases from root to tip of the blade, for the exhaust gas flow is diverted to tip side of the propeller blade. However, the optimized duct was found satisfactory at given flight operating conditions and the same duct will be further used for flight testing.

This paper discusses some of the many variations in exhaust stub design, and examines how they influence the performance of the engine, the performance of the aircraft, and the manufacturing aspect. A detailed analysis was performed on the influencing parameters, such as the location, orientation, flange dimension, and geometric effective area, of exhaust port.

2. Sizing of Exhaust Stub

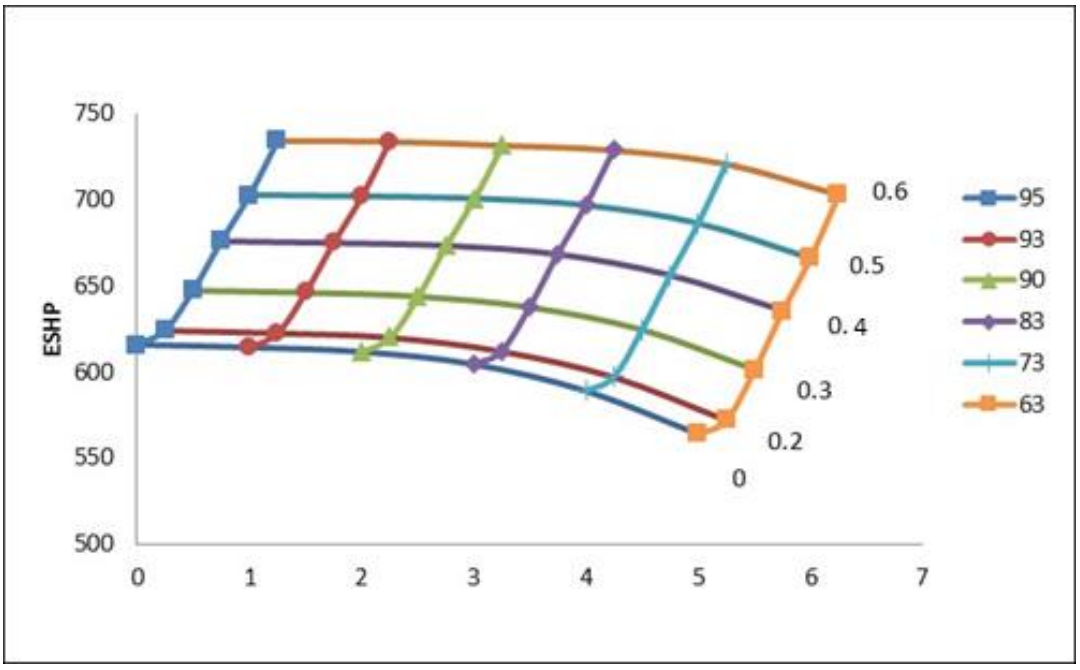

Figure 3. Stub area studies. Installed case, altitude: 30,000 ft, ISA+15
(Power rating: Max. cruise)

Figure 3 presents a carpet plot of ESHP as a function of free stream Mach number and effective stub exit area generated by the estimated engine performance program (EEPP) in the installed condition at 30,000 ft, ISA+15°C and maximum cruise rating. The ESHP can be calculated by:

$$ESHP = SHP + \frac{FN \times TAS \times 1.688}{550 \times \eta prop} \quad (1)$$

where, FN is net exhaust gas thrust, lb; TAS is true air velocity, knots; 1.688 is the conversion factor from knots to feet/second; 550 is the conversion factor from SHP to lb-feet/second; $\eta prop$ is the propeller efficiency.

As shown in Figure 3, the effect of stub area is not significant at higher Mach numbers in terms of ESHP. The ESHP does not change significantly beyond 90 in^2 at all Mach numbers.

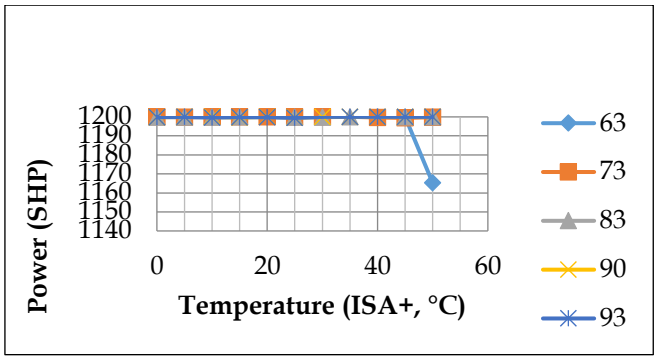

Figure 4. Stub area studies. Installed case, Altitude: Sea level (Power rating: Max. take off)

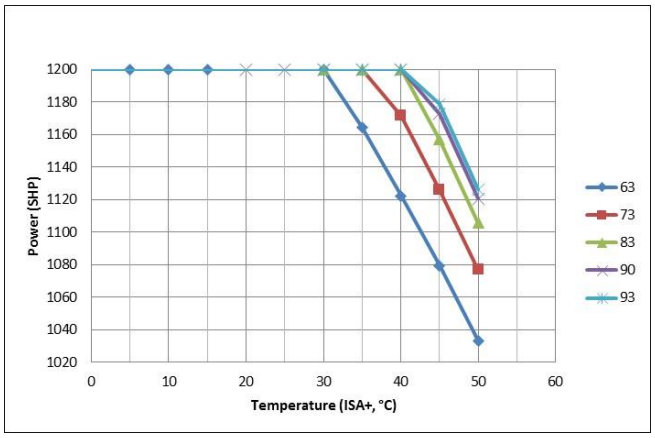

Figure 5. Stub area studies. Installed case, Altitude: 2 km (Power rating: Max. take off)

Figures 4 and 5 show the SHP variation with temperature changing from ISA to ISA+50°C and with stub exit area at sea level and 2 km altitude, respectively. It can be seen that, with an effective stub area of 93 in^2, it is possible to get full power of 1200 SHP up to ISA+40°C at sea level. By contrast, with 93 in^2 stub area at ISA+45°C, there is a drop of about 6 SHP. At ISA+50°C, the decline is about 5 SHP at 2 km altitude.

In the case of single engine failure, the full power should be produced by the other engine. This is the only way to meet the single climb gradient required by FAR23 [10]. Thus, the effective area could be selected as in^2. As per the installation manual, the typical stub flow coefficients are of the order of 0.85. Therefore, the geometric area for the stub would be 93/0.85 = 109.4 in^2. Since the geometric area of the exhaust duct port, 109.4 in^2 (54.70 in^2 per side), is slightly larger than the engine flange area (54.62 in^2), the resulting stub will be relatively simple to design aerodynamically.

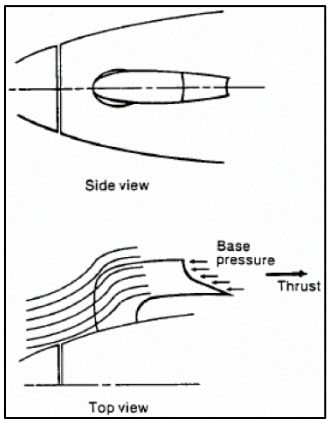

Figure 6. Exhaust stub – full turning contoured stub

The stub exit could be elliptical with the cutback angle. Figure 6 shows a good exhaust duct design with longer cutback length, which favors flow turning at the inner radius, and thus improves performance for aircraft configuration. To design exhaust stubs for different aircrafts, special attention should be paid to the exhaust stub angle, for hot exhaust gas would impinge on aircraft surfaces and structures, and exhaust stubs should not create any additional external aerodynamic drag [11-15].

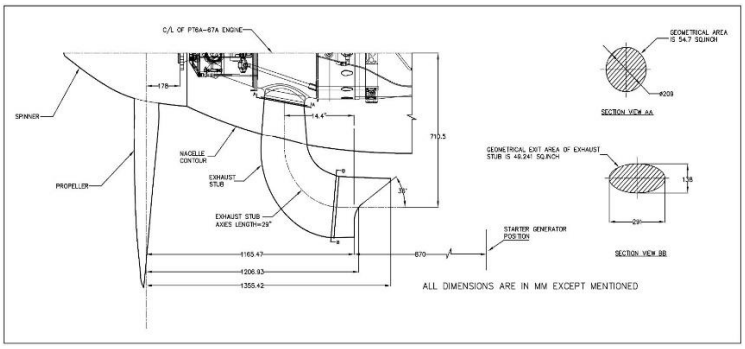

Note: Specific dimensions:
a. Exhaust stub axial length = 29 inches.
b. Geometrical area = 54.7 Sq. inch.
c. Geometrical exit area of exhaust stub = 49.241 Sq. inch.
d. Cut back angle = 36°.

Figure 7. Exhaust stub – full turning contoured stub

The design of internal flow ducts should minimize the pressure loss induced by the flow separation from the internal walls of the duct. For this purpose, a small turning angle needs to be adopted. According to external drag considerations, a fully turning with the faired stub has the least drag. As a design compromise, this research selects the stub with full turning faired with cut back angle (Figure 7).

3. Profile of Exhaust Temperature

Based on the above stub design, the variation of the exhaust jet temperature (at stub exit, T_7) with velocity and altitude at maximum cruise rating is illustrated in Figure 8. At a given distance from the exhaust stub exit plane, the jet temperature can be estimated in the following manner.

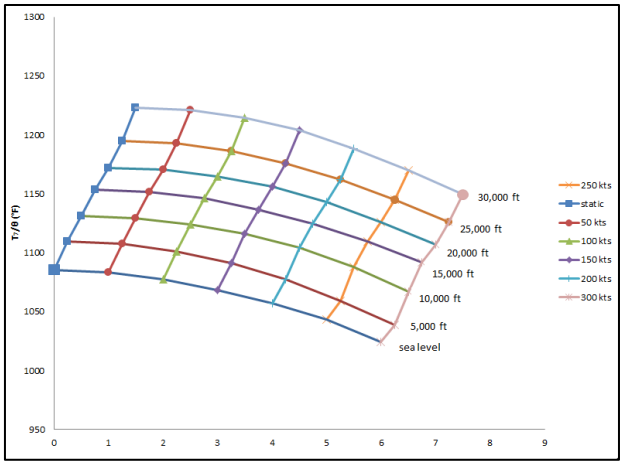

Figure 8. Variation of the exhaust jet temperature (at stub exit) with velocity and altitude at ISA+25

3.1 Engine exhaust exist plane

3.1.1 Static condition (V1/V7 = 0)

The distance of exhaust exit plane from stub exit plane (L) is 366 mm and the stub diameter (d_7) is 209 mm. Therefore, $L/d_7 = 366/209 = 1.75$. Figure 9 presents the exhaust jet temperature profile as a function of exhaust velocity ratio (relative to free stream). Note that the temperature profile is based on one-dimensional analysis,

which excludes free stream inflow effects due to aircraft pitch, yaw and propeller swirl. It can be seen from Figure 9 that:

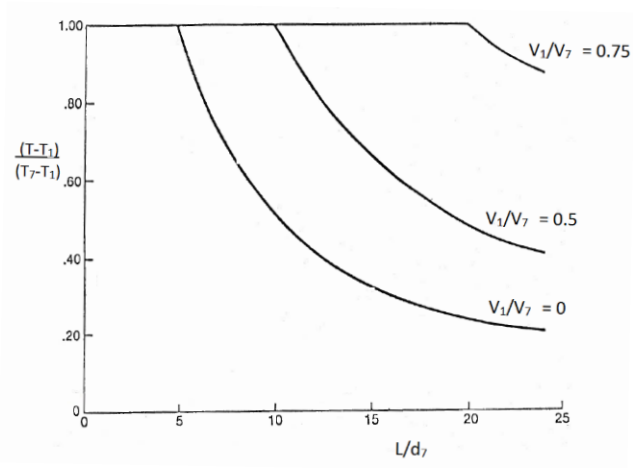

Figure 9. Exhaust jet temperature profile

The distance of exhaust exit plane from stub exit plane (L) is 366 mm and the stub diameter (d_7) is 209 mm. Therefore, $L/d_7 = 366/209 = 1.75$. Figure 9 presents the exhaust jet temperature profile as a function of exhaust velocity ratio (relative to free stream). Note that the temperature profile is based on one-dimensional analysis, which excludes free stream inflow effects due to aircraft pitch, yaw and propeller swirl. It can be seen from Figure 9 that:

$$(T\text{-}T_1)/(T_7\text{-}T_1) = 1 \quad (2)$$

where, T is the local temperature of exhaust jet; T_1 is the air temperature of free stream; T_7 is the exhaust jet temperature at stub exit.

As shown in Figure 8, at static, sea level, ISA+25°C condition, we have $T_7/\theta = 1087$°F. The free stream air temperature $T_1 = 40$°C = 104°F. Hence,

$$\theta = \frac{(T_1+460)}{518.7} = 1.09 \quad (3)$$

3.1.2 Cruise condition (V1/V7 = 1.2)

For cruise condition, $V_1/V_7 = 1.2$ and for the same $L/d_7 = 1.75$ and $(T\text{-}T_1)/(T_7\text{-}T_1) = 1$ as before. As shown in Figure 8, we have $T_7/\theta = 1149$ °F at M = 0.5 (300 kts) at 30,000 ft and ISA +25°C. In this case, the free stream air temperature, $T_1 = 29$°F. Hence, $\theta = \frac{(T_1+460)}{518.7} = 0.94$. Therefore, $T_7 = T = 1080$°F.

For the proposed exhaust stubs, the jet temperatures at engine stub exit T_7 and local temperature at exhaust stub exit plane T for both static and cruise conditions are 1184 (640°C) and 1080°F (582°C), respectively.

3.2 Midsection of Nacelle

3.2.1 Static condition (V1/V7 = 0)

The distance of midsection of nacelle from stub exit plane (L) is 1236 mm and the stub diameter (d_7) is 209 mm. Therefore, $L/d_7 = 1236/209 = 5.9$; $(T\text{-}T_1)/(T_7\text{-}T_1) = 0.9$. As shown in Figure 8, at static, sea level, ISA+25°C condition, we have $T_7/\theta = 1087$°F. The free stream air temperature $T_1 = 40$°C = 104°F. Hence, $\theta = \frac{(T_1+460)}{518.7} = 1.09$. Therefore, $T_7 = 1184$°F and T = 1076°F.

3.2.2 Cruise condition (V1/V7 = 1.2)

For cruise condition, $V_1/V_7 = 1.2$ and for the same $L/d_7 = 5.9$ and $(T\text{-}T_1)/(T_7\text{-}T_1) = 0.9$ as before. $T_7/\theta = 1149$ °F at M = 0.5 (300 kts) at 30,000 ft and ISA +25°C. In this case, the free stream air temperature, $T_1 = 29$°F. Hence, $\theta = \frac{(T_1+460)}{518.7} = 0.94$. Therefore, $T_7 = 1080$°F and T = 982°F.

The local temperature of exhaust jet near nacelle midsection is 1076°F (580°C) for the static condition, and for cruise condition 982°F (527°C).

4. Discussion

Thermal IR and CFD were performed on the proposed exhaust stub design. The engine exhaust temperature along the exit plane was measured by thermal IR during the EGR (Engine Ground Run, for the static reverse condition). The comparative results in Figure 10 suggest that our method and numerical model are satisfactory, and the proposed exhaust stub design can be implemented on aircraft.

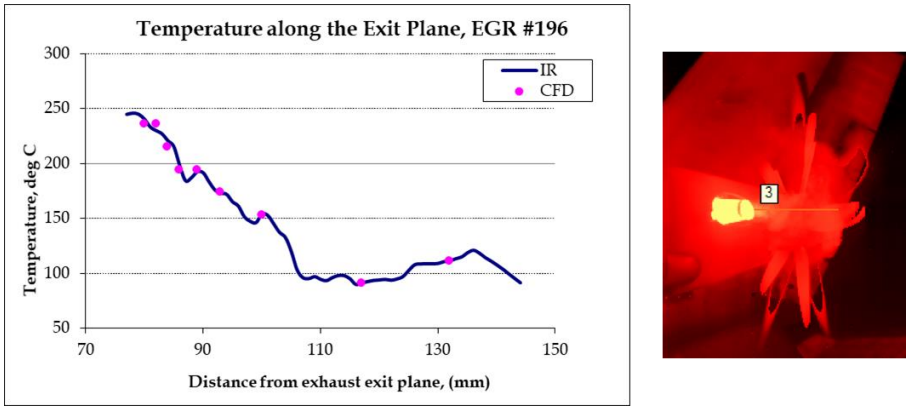

Figure 10. Comparison of thermal IR and CFD results of temperature along the exit plane

5. Conclusions

This paper discusses the main design considerations for the exhaust stub (or nozzle) design for the LTA fitted with a twin port exhaust case, and explores how the select effective exit area of the stub and exit distance. It was found that the stub exit could be elliptical with the cutback angle. As a good exhaust design with longer cutback length will favor flow turning at the inner radius, which would improve the performance for aircraft configuration. The exit distance is the minimum distance, measured at the exit plane of the stub, between the aircraft cowling and the exhaust stub. Minimizing this distance could reduce the load on the engine exhaust flange. The stubs need to be turned to maximize thrust recovery, minimize the effect of external aerodynamic drag, and avoid problems arising from overheating of aircraft surfaces and sooting.

Table 1. Temperature of exhaust stub at static and cruise conditions

Serial number	Flight condition	Location		
		Engine stub exit temperature (T_7) °F (°C)	Exhaust stub exit plane °F (°C)	Local plane exhaust jet temperature (Nacelle midsection) °F (°C)
1.	Static	1184 (640)	1184 (640)	1076 (580)
	Cruise	1080 (582)	1080 (582)	982 (527)

In addition, the jet temperature at exhaust stub exit (T_7) and temperature at exhaust stub exit plane and nacelle midsection were determined at both static and cruise conditions (Table 1). The relevant data can serve as boundary conditions for CFD/thermal analysis of exhaust temperature effects on the nacelle and aircraft surfaces.

Data Availability

The data used to support the findings of this study are available from the corresponding author upon request.

Acknowledgements

The authors would like to thank all partners for their contribution to this program and for their permission to publish this paper.

Conflicts of Interest

The authors declare that they have no conflicts of interest.

References

[1] P. Lathasree and A. A. Pashilkar, "Digital simulation model for turboprop engine," In Proceedings of Symposium on Applied Aerodynamics and Design of Aerospace Vehicle, (SAROD 2011), Bangalore, India, November 16-18, 2011, SAROD, pp. 1-6.

[2] P. Guła, D. Ulma, K. Żurek, and R. Żurawski, "Challenges of turboprop engine installation on small aircraft," *Aircr. Eng. Aerosp. Tec.*, vol. 91, no. 7, pp. 938-948, 2019. http://dx.doi.org/10.1108/AEAT-09-2017-0198

[3] C. Kong, "Propulsion system Integration of turboprop aircraft for basic trainer," *Aircr. Eng. Aerosp. Tec.*, vol. 72, no. 6, pp. 524-537, 2000. http://dx.doi.org/10.1108/00022660010357486.

[4] W. Stalewski, "Design and optimisation of exhaust system of light turboprop airplane," *J. KONES*, vol. 23, no. 2, pp. 341-348, 2016. http://dx.doi.org/10.5604/12314005.1213748.

[5] D. C. Wilcox, "A two-equation turbulence model for wall-bounded and free-shear flows," AIAA Journal, vol. 1993, 1993.

[6] D. C. Wilcox, "Turbulence modeling for CFD," cfd, 1998, https://cfd.spbstu.ru/agarbaruk/doc/2006_Wilcox_Turbulence-modeling-for-CFD.pdf.

[7] "Ansys Fluent User's Guide, Release 15.0," ANSYS, 2013, http://www.ansys.com.

[8] "Ansys Fluent Theory Guide, Release 15.0," ANSYS, 2013, http://www.ansys.com.

[9] M. Mali, C. Vinay, and S. V. Kadam, "Numerical analysis of propeller blade temperature for optimized stub of pusher configured turboprop aircraft," *IJIRSET*, vol. 7, no. 4, pp. 3444-3451, 2018. http://dx.doi.org/10.15680/IJIRSET.2018.0704035.

[10] "US Department of Transportation, Federal Aviation Administration", Federal Aviation Administration, 1912, https://www.faa.gov.

[11] C. A. Vinay, K. G. Narayanappa, and Y. G. Babu, "Experimental and numerical investigation on the effect of turboprop engine exhaust gas impingement on pusher aircraft," *Int. J. Turbo Jet-Eng.*, vol. 2022, 2022. https://doi.org/10.1515/tjj-2022-0011.

[12] C. A. Vinay and G. N. Kumar, "Aero-thermal investigation of thermal interactions between turboprop engine exhaust and selected parts of the airplane skin for tractor configured aircraft," *Aircr. Eng. Aerosp. Tec.,* vol. 95, no. 2, pp. 594-606, 2022. http://dx.doi.org/10.1108/AEAT-03-2022-0082.

[13] C. A. Vinay and B. Chakravarthy, "Aerothermal analysis of insulation to protect exhaust ducts of a pusher turbo prop engine aircraft," *In Fluid Mechanics and Fluid Power–Contemporary Research,* Heidelberg, Berlin: Springer, pp. 843-851, 2017. https://doi.org/10.1007/978-81-322-2743-4_79.

[14] Z. H. Xie and S. Wu, "Thermal effect analysis of engine exhaust jet flow on the structures of a carrier-based airborne early-warning aircraft," In the 2016 World Congress on Advances in Civil, Environmental, and Materials Research, Jeju Island, Korea, 2016, ACEM, pp. 1-9.

[15] P. Łapka, M. Seredyński, and P. Furmański, "Investigation of thermal interactions between the exhaust jet and airplane skin in small aircrafts," *Progress in Computational Fluid Dynamics an Int J.*, vol. 19, no. 1, pp. 35-43, 2019. http://dx.doi.org/10.1504/PCFD.2019.097596